

A multiscale reduced basis method for Schrödinger equation with multiscale and random potentials

Jingrun Chen^a, Dingjiong Ma^b, Zhiwen Zhang^{b,*}

^a*Mathematical Center for Interdisciplinary Research and School of Mathematical Sciences, Soochow University, Suzhou, China.*

^b*Department of Mathematics, The University of Hong Kong, Pokfulam Road, Hong Kong SAR, China.*

Abstract

The semiclassical Schrödinger equation with multiscale and random potentials often appears when studying electron dynamics in heterogeneous quantum systems. As time evolves, the wavefunction develops high-frequency oscillations in both the physical space and the random space, which poses severe challenges for numerical methods. In this paper, we propose a multiscale reduced basis method, where we construct multiscale reduced basis functions using an optimization method and the proper orthogonal decomposition method in the physical space and employ the quasi-Monte Carlo method in the random space. Our method is verified to be efficient: the spatial gridsize is only proportional to the semiclassical parameter and the number of samples in the random space is inversely proportional to the same parameter. Several theoretical aspects of the proposed method, including how to determine the number of samples in the construction of multiscale reduced basis and convergence analysis, are studied with numerical justification. In addition, we investigate the Anderson localization phenomena for Schrödinger equation with correlated random potentials in both 1D and 2D.

Keyword: random Schrödinger equation; multiscale reduced basis function; optimization method; quasi-Monte Carlo method; Anderson localization.

AMS subject classifications. 35J10, 35Q41, 65M60, 65K10, 74Q10.

1. Introduction

The semiclassical Schrödinger equation describes electron dynamics in the semiclassical regime. Applications of such an equation can be found in Bose-Einstein condensation, graphene, semiconductors, topological insulators, etc. When propagating in a (quasi-)periodic microstructure, electrons experience a multiscale potential. As a consequence, the electron wavefunction develops high-frequency oscillations, which poses severe challenges from the numerical perspective. Brute-force methods are very costly and asymptotics-based methods have been proposed in the literature; see [26] for review and references therein.

*Corresponding author

Email addresses: jingrunchen@suda.edu.cn (Jingrun Chen), martin35@hku.hk (Dingjiong Ma), zhangzw@hku.hk (Zhiwen Zhang)

In [2], Anderson proposed to study localized eigenstates in a tight-binding model with random potentials. This model was soon to be generalized to the random Schrödinger equation, i.e., the Schrödinger equation with a random potential. In this case, electrons are found to be localized provided that the strength of randomness is sufficiently large. The randomness can be realized in an experiment by enhancing the disorder of impurities in a material. Due to the importance of this model, Anderson was awarded the Nobel Prize in physics in 1977. In the presence of multiscale and random potentials, the electron wavefunction develops high-frequency oscillations in both the physical space and the random space, making numerical approximations even more difficult.

In this paper, we study the following Schrödinger equation with random potential in the semiclassical regime

$$\begin{cases} i\varepsilon\partial_t\psi^\varepsilon = -\frac{\varepsilon^2}{2}\Delta\psi^\varepsilon + v^\varepsilon(\mathbf{x},\omega)\psi^\varepsilon, & \mathbf{x} \in D, \quad \omega \in \Omega, \quad t \in \mathbb{R}, \\ \psi^\varepsilon \in H_P^1(D), & \omega \in \Omega, \quad t \in \mathbb{R}, \\ \psi^\varepsilon|_{t=0} = \psi_{\text{in}}(\mathbf{x}), & \mathbf{x} \in D, \end{cases} \quad (1)$$

where $0 < \varepsilon \ll 1$ is an effective Planck constant describing the microscopic and macroscopic scale ratio, d is the spatial dimension, $v^\varepsilon(\mathbf{x},\omega)$ is the given random potential, $\psi^\varepsilon = \psi^\varepsilon(t, \mathbf{x}, \omega)$ is the electron wavefunction, and $\psi_{\text{in}}(\mathbf{x})$ is the initial data. Here $D = [0, 1]^d$ is the spatial domain and $H_P^1(D) = \{\psi | \psi \in H^1(D) \text{ and } \psi \text{ is periodic over } D\}$.

Equation (1) can be used to model electron transport in a disordered medium in a single-electron picture where the electron interaction is ignored. It is customary to write the semiclassical Schrödinger equation and the multiscale and random potential with a single parameter ε . But there is no reason that the parameter of the multiscale and random potential should be the same as the semiclassical parameter; see §5 for details on the parameterization of the multiscale and random potential $v^\varepsilon(\mathbf{x},\omega)$.

The existence of Anderson localization is closely related to the electron wavefunction in (1). To be specific, assume $\psi^\varepsilon(t, \mathbf{x}, \omega)$ has zero mean with respect to the measure ρ induced by $v^\varepsilon(\mathbf{x},\omega)$ and denote $A(t) = \mathbb{E}[\int_{R^d} |\mathbf{x}|^2 |\psi^\varepsilon|^2 d\mathbf{x}]_\rho$ the second-order moment of the position density. When the strength of disorder is small, an electron undergoes a diffusion process with $A(t) = 2C_d t$, $C_d > 0$. In the presence of a strong disorder, however, $A(t)$ converges to a time-independent quantity, i.e., $\lim_{t \rightarrow \infty} A(t) = C$, which implies the localization of the electron and the system undergoes a metal-insulator transition [32, 14]. When $d = 1$, localization always occurs for (1) with random potential [2]. When $d \geq 2$, the situation becomes complicated. Some analytical results show that localization occurs when the strength of disorder is large [18, 1]. This motivates us to study Anderson localization in the presence of correlated random potentials [34].

When the potential is deterministic, i.e., $v^\varepsilon(\mathbf{x},\omega) = v^\varepsilon(\mathbf{x})$, many numerical methods have been proposed; see [4, 16, 39, 27, 15, 9, 8] for example. When the potential is random, few works have been done; see [40, 25]. As mentioned above, the major difficulty is that the wavefunction ψ^ε develops high-frequency oscillations in both the physical space and the random space, which requires tremendous computational resources.

Our work is motivated by the multiscale finite element method (FEM) for solving elliptic problems with multiscale coefficients [21, 13]. The multiscale FEM is capable of correctly capturing the large scale components of the multiscale solution on a coarse grid without accurately resolving all the small scale features in the solution. This is accomplished by incorporating the local microstructures of the differential operator into the multiscale FEM basis functions. Recently, several relevant works on constructing localized basis functions that approximate the elliptic operator with heterogeneous coefficients have been proposed. In [31], Malqvist and Peterseim construct localized multiscale basis functions using a modified variational multiscale method. The exponentially decaying property of these modified basis has been shown both theoretically and numerically. Meanwhile, Owhadi [35, 36] reformulates the multiscale problem from the perspective of decision theory using the idea of gamblets as the modified basis. Hou et.al. [24] extend these works such that localized basis functions can also be constructed for higher-order strongly elliptic operators. Recently, Hou, Ma, and Zhang propose to build localized multiscale stochastic basis to solve elliptic problems with multiscale and random coefficients [22].

In this paper, we propose a multiscale reduced basis method to solve the Schrödinger equation with random potentials in the semiclassical regime. Our method consists of offline and online stages. In the offline stage, we apply an optimization approach to systematically construct localized multiscale reduced basis functions on each patch associated with each coarse gridpoint. These basis functions provide nearly optimal approximation to the random Schrödinger operator. In the online stage, we use these basis functions to approximate the physical space of the solution and the quasi-Monte Carlo (qMC) method to approximate the random space of the solution, respectively. We find the proposed method is efficient in the sense that the number of basis functions is only proportional to ε and the number of samples in qMC is inversely proportional to ε . Under some conditions, we conduct the convergence analysis of the proposed method with numerical verifications. Moreover, we study how to determine the number of samples in qMC such that the corresponding multiscale reduced basis functions provide accurate approximation of the solution space. Finally we investigate the existence of Anderson localization for correlated random potentials.

The rest of the paper is organized as follows. For completeness, in §2, we introduce multiscale basis functions for the deterministic Schrödinger equation in semiclassical regime and discuss some properties of the basis functions. In §3, we propose a multiscale reduced basis method to solve the random Schrödinger equation. Analysis results are presented in §4 and numerical experiments, including both 1D and 2D examples, are conducted to demonstrate the convergence and efficiency of the proposed method in §5. Conclusions and discussions are drawn in §6.

2. Multiscale basis functions for deterministic Schrödinger equations

In this section, we briefly review the construction of multiscale basis functions based on an optimization approach to solve the Schrödinger equation with a deterministic potential. Some properties of the multiscale basis functions are also given.

2.1. Construction of multiscale basis functions

In the deterministic case, we consider the following problem

$$\begin{cases} i\varepsilon\partial_t\psi^\varepsilon = -\frac{\varepsilon^2}{2}\Delta\psi^\varepsilon + v^\varepsilon(\mathbf{x})\psi^\varepsilon, & \mathbf{x} \in D, \quad t \in \mathbb{R}, \\ \psi^\varepsilon \in H_{\mathbb{P}}^1(D), \\ \psi^\varepsilon|_{t=0} = \psi_{\text{in}}(\mathbf{x}). \end{cases} \quad (2)$$

$\psi_{\text{in}}(\mathbf{x})$ is the initial data over D . Defining the Hamiltonian operator $\mathcal{H}(\cdot) \equiv -\frac{\varepsilon^2}{2}\Delta(\cdot) + v^\varepsilon(\mathbf{x})(\cdot)$ and introducing the following energy notation $\|\cdot\|_V$ for Hamiltonian operator

$$\|\psi^\varepsilon\|_V = \frac{1}{2}(\mathcal{H}\psi^\varepsilon, \psi^\varepsilon) = \frac{1}{2} \int_D \frac{\varepsilon^2}{2} |\nabla\psi^\varepsilon|^2 + v^\varepsilon(\mathbf{x})|\psi^\varepsilon|^2 d\mathbf{x}. \quad (3)$$

Note that (3) does not define a norm since v^ε usually can be negative, and thus the bilinear form associated to this notation is not coercive, which is quite different from the case of elliptic equations. However, this does not mean that available approaches [23, 3, 31, 36, 24] cannot be used for the Schrödinger equation. In fact, we shall utilize the similar idea to construct localized multiscale basis functions on a coarse mesh by an optimization approach using the above energy notation $\|\cdot\|_V$ for the Hamiltonian operator.

To construct such localized multiscale basis functions, we first partition the physical domain D into a set of regular coarse elements with mesh size H . For example, we divide D into a set of non-overlapping triangles $\mathcal{T}_H = \cup\{K\}$, such that no vertex of one triangle lies in the interior of the edge of another triangle. On each element K , we define a set of nodal basis $\{\varphi_{j,K}, j = 1, \dots, k\}$ with k being the number of nodes of the element. From now on, we neglect the subscript K for notational convenience. The functions $\varphi_i(\mathbf{x})$ are called measurement functions, which are chosen as the characteristic functions on each coarse element in [24, 36] and piecewise linear basis functions in [31]. In [29, 22], it is found that the usage of FEM nodal basis functions reduces the approximation error and thus the same setting is adopted in the current work.

Let \mathcal{N} denote the set of vertices of \mathcal{T}_H (removing the repeated vertices due to the periodic boundary condition) and N_H be the number of vertices. For every vertex $\mathbf{x}_i \in \mathcal{N}$, let $\varphi_i^H(\mathbf{x})$ denote the corresponding nodal basis function, i.e., $\varphi_i^H(\mathbf{x}_j) = \delta_{ij}$. Since all the nodal basis functions $\varphi_i(\mathbf{x})$ are continuous across the boundaries of the elements, we have

$$V^H = \{\varphi_i^H(\mathbf{x}) : i = 1, \dots, N_H\} \subset H_{\mathbb{P}}^1(D).$$

Then, we can solve optimization problems to obtain the multiscale basis functions. Specifically, let $\phi_i(\mathbf{x})$ be the minimizer of the following constrained optimization problem

$$\phi_i = \arg \min_{\phi \in H_{\mathbb{P}}^1(D)} \|\phi\|_V \quad (4)$$

$$\text{s.t. } \int_D \phi \varphi_j^H d\mathbf{x} = \delta_{i,j}, \quad \forall 1 \leq j \leq N_H. \quad (5)$$

The superscript ε is dropped for notation simplicity and the periodic boundary condition is incorporated into the above optimization problem through the solution space $H_{\text{p}}^1(D)$.

In general, one cannot solve the above optimization problem analytically. Therefore, we use numerical methods to solve it. Specifically, we partition the physical domain D into a set of non-overlapping fine triangles with size $h \ll \varepsilon$. Then, we use standard FEM to discretize $\phi_i(\mathbf{x})$, $\varphi_j^H(\mathbf{x})$, $1 \leq i, j \leq N_H$. In the discrete level, the optimization problem (4)-(5) is reduced to a constrained quadratic optimization problem; see (19) in Section 3.3, which can be efficiently solved using Lagrange multiplier methods. Finally, with these multiscale FEM basis functions $\{\phi_i(\mathbf{x})\}_{i=1}^{N_H}$, we can solve the Schrödinger equation (2) using the Galerkin method.

Remark 2.1. In analogy to the multistate FEM [21, 13], the multiscale basis functions $\{\phi_i(\mathbf{x})\}_{i=1}^{N_H}$ are defined on coarse elements with mesh size H . However, they are represented by fine-scale FEM basis with mesh size h , which can be pre-computed and done in parallel.

Remark 2.2. The notation $\|\cdot\|_V$ in (3) does not define a norm. However, as long as the potential $v^\varepsilon(\mathbf{x})$ is bounded from below and the fine mesh size h is small enough, the discrete problem of (4) - (5) is convex and thus admits a unique solution; see [24, 29] for details.

2.2. Exponential decay of the multiscale finite element basis functions

It can be proved that the multiscale basis functions $\{\phi_i(\mathbf{x})\}_{i=1}^{N_H}$ decay exponentially fast away from its associated vertex $\mathbf{x}_i \in \mathcal{N}_c$ under certain conditions. This allows us to localize the basis functions to a relatively smaller domain and reduce the computational cost. We first define a series of nodal patches $\{D_\ell\}$ associated with $\mathbf{x}_i \in \mathcal{N}$ as

$$D_0 := \text{supp}\{\varphi_i\} = \cup\{K \in \mathcal{T}_H | \mathbf{x}_i \in K\}, \quad (6)$$

$$D_\ell := \cup\{K \in \mathcal{T}_H | K \cap \overline{D_{\ell-1}} \neq \emptyset\}, \quad \ell = 1, 2, \dots. \quad (7)$$

Assumption 2.1. *We assume the potential $v^\varepsilon(\mathbf{x})$ is bounded, i.e., $V_0 := \|v^\varepsilon(\mathbf{x})\|_{L^\infty(D)} < +\infty$ and the mesh size H of \mathcal{T}_H satisfies*

$$\sqrt{V_0}H/\varepsilon \lesssim 1, \quad (8)$$

where \lesssim means bounded from above by a constant.

Under this resolution assumption for the coarse mesh, many typical potentials in the Schrödinger equation (2) can be treated as a perturbation to the kinetic operator. Thus, they can be computed using our method. Then, we can show that the multiscale finite element basis functions have the exponentially decaying property.

Proposition 2.2 (Exponentially decaying property). *Under the resolution condition of the coarse mesh, i.e., (8), there exist constants $C > 0$ and $0 < \beta < 1$ independent of H , such that*

$$\|\nabla\phi_i(\mathbf{x})\|_{L^2(D \setminus D_\ell)} \leq C\beta^\ell \|\nabla\phi_i(\mathbf{x})\|_{L^2(D)}, \quad (9)$$

for any $i = 1, 2, \dots, N_H$.

Proof of (9) will be given in [7]. The main idea is to combine an iterative Caccioppoli-type argument [31, 29] and some refined estimates with respect to ε .

The exponential decay of the basis functions enables us to localize the support sets of the basis functions $\{\phi_i(\mathbf{x})\}_{i=1}^{N_H}$, so that the corresponding stiffness matrix is sparse and the computational cost is reduced. In practice, we define a modified constrained optimization problem as follows

$$\phi_i^{\text{loc}} = \arg \min_{\phi \in H_P^1(D)} \|\phi\|_V \quad (10)$$

$$\text{s.t.} \quad \int_{D_{l^*}} \phi \varphi_j^H \, d\mathbf{x} = \delta_{i,j}, \quad \forall 1 \leq j \leq N_H, \quad (11)$$

$$\phi(\mathbf{x}) = 0, \quad \mathbf{x} \in D \setminus D_{l^*}, \quad (12)$$

where D_{l^*} is the support set of the localized multiscale basis function $\phi_i^{\text{loc}}(\mathbf{x})$ and the choice of the integer l^* depends on the decaying speed of $\phi_i^{\text{loc}}(\mathbf{x})$. In (11) and (12), we have used the fact that $\phi_i(\mathbf{x})$ has the exponentially decaying property so that we can localize the support set of $\phi_i(\mathbf{x})$ to a smaller domain D_{l^*} . In numerical experiments, we find that a small integer $l^* \sim \log(L/H)$ will give accurate results, where L is the diameter of domain D . Moreover, the optimization problem (10)-(12) can be solved in parallel. Therefore, the exponentially decaying property significantly reduces our computational cost in constructing basis functions and computing the solution of the Schrödinger equation (2).

With the localized multiscale finite element basis functions $\{\phi_i^{\text{loc}}(\mathbf{x})\}_{i=1}^{N_H}$, we can approximate the wavefunction by $\psi^\varepsilon(\mathbf{x}, t) = \sum_{i=1}^{N_H} c_i(t) \phi_i^{\text{loc}}(\mathbf{x})$ using the Galerkin method.

3. Multiscale reduced basis functions for the random Schrödinger equation

3.1. Parametrization of the random potential

The random potential $v^\varepsilon(\mathbf{x}, \omega)$ is used to model the disorder in a given material. Specifically, we assume $v^\varepsilon(\mathbf{x}, \omega)$ is a second order random field, i.e., $v^\varepsilon(\mathbf{x}, \omega) \in L^2(D, \Omega)$, with mean $\mathbb{E}[v^\varepsilon(\mathbf{x}, \omega)] = \bar{v}^\varepsilon(\mathbf{x})$ and covariance kernel $C(\mathbf{x}, \mathbf{y})$. For example, we can choose the covariance kernel as

$$C(\mathbf{x}, \mathbf{y}) = \sigma^2 \exp\left(-\sum_{i=1}^d \frac{|x_i - y_i|^2}{2l_i^2}\right), \quad (13)$$

where σ is a constant and l_i 's are the correlation lengths in each dimension. We also assume that the random potential $v^\varepsilon(\mathbf{x}, \omega)$ is almost surely bounded, namely there exist v_{\max} and v_{\min} , such that

$$P(\omega \in \Omega \mid v^\varepsilon(\mathbf{x}, \omega) \in [v_{\min}, v_{\max}], \quad \forall \mathbf{x} \in D) = 1. \quad (14)$$

Circulant embedding method [12] and Karhunen-Loève (KL) expansion method [28, 30] are commonly used to generate samples of $v^\varepsilon(\mathbf{x}, \omega)$, and the latter will be used in the current work.

The KL expansion of $v^\varepsilon(\mathbf{x}, \omega)$ reads as

$$v^\varepsilon(\mathbf{x}, \omega) = \bar{v}^\varepsilon(\mathbf{x}) + \sum_{i=1}^{\infty} \sqrt{\lambda_i} \xi_i(\omega) v_i(\mathbf{x}), \quad (15)$$

where $\xi_i(\omega)$'s are mean-zero and uncorrelated random variables, i.e., $\mathbb{E}[\xi_i] = 0$, $\mathbb{E}[\xi_i \xi_j] = \delta_{ij}$, and $\{\lambda_i, v_i(\mathbf{x})\}_{i=1}^{\infty}$ are the eigenpairs of the covariance kernel $C(\mathbf{x}, \mathbf{y})$. Generally, λ_i 's are sorted in a descending order and their decay rates depend on the regularity of the covariance kernel. It has been proven that an algebraic decay rate, i.e. $\lambda_i = \mathcal{O}(i^{-\gamma})$, is achieved asymptotically if the covariance kernel is of finite Sobolev regularity, and an exponential decay rate is achieved, i.e., $\lambda_i = \mathcal{O}(e^{-\gamma i})$ for some $\gamma > 0$, if the covariance kernel is piecewisely analytic [37].

In practice, we truncate the KL expansion (15) into its first m terms and obtain a parametrization of the random potential as

$$v_m^\varepsilon(\mathbf{x}, \omega) = \bar{v}^\varepsilon(\mathbf{x}) + \sum_{i=1}^m \sqrt{\lambda_i} \xi_i(\omega) v_i(\mathbf{x}), \quad (16)$$

which will be used in both analysis and numerics in the remaining part of the paper.

Remark 3.1. In general, the decay rate of λ_i depends on the correlation lengths l_i , $i = 1, \dots, d$ of the random field $v^\varepsilon(\mathbf{x}, \omega)$. Small correlation length results in slow decay of the eigenvalues. When the correlation lengths approach zero, the random field $v^\varepsilon(\mathbf{x}, \omega)$ becomes a spatially white noise, which is the case used in the original physics paper [2].

3.2. Construction of the multiscale reduced basis functions

For the random Schrödinger equation (1), it is prohibitively expensive to construct multiscale basis functions for each realization of the random potential using (10) - (12). To address this issue, we use a model reduction method to build a small number of reduced basis functions that enable us to obtain multiscale basis functions in a cheaper way without loss of approximation accuracy.

For every $\mathbf{x}_k \in \mathcal{N}$, we first compute a set of samples of multiscale basis functions associated to the vertex \mathbf{x}_k . Specifically, let $\{v^\varepsilon(\mathbf{x}, \omega_q)\}_{q=1}^Q$ be samples of the random potential that are obtained using Monte Carlo (MC) method or qMC method, where Q is the number of samples. Denote $\zeta_0^k(\mathbf{x}) = \frac{1}{Q} \sum_{q=1}^Q \phi_k^{\text{loc}}(\mathbf{x}, \omega_q)$ the sample mean of the basis functions, and $\tilde{\phi}_k^{\text{loc}}(\mathbf{x}, \omega_q) = \phi_k^{\text{loc}}(\mathbf{x}, \omega_q) - \zeta_0^k(\mathbf{x})$ is the fluctuation of the k -th basis function.

We apply the proper orthogonal decomposition (POD) method [5, 38] to $V = \{\tilde{\phi}_k^{\text{loc}}(\mathbf{x}, \omega_q)\}_{q=1}^Q$ and build a set of basis functions $\{\zeta_1^k(\mathbf{x}), \zeta_2^k(\mathbf{x}), \dots, \zeta_{m_k}^k(\mathbf{x})\}$ with $m_k \ll Q$ that optimally approximates V . Quantitatively, we have the following approximating property.

Proposition 3.1. *Let $\lambda_1 \geq \lambda_2 \geq \dots \geq \lambda_{m_k} \geq \lambda_{m_k+1} \geq \dots > 0$ be positive eigenvalues of the covariance kernel associated with the snapshot of the fluctuations V and the corresponding eigenfunctions are $\zeta_1^k(\mathbf{x}), \dots, \zeta_{m_k}^k(\mathbf{x}), \dots$. Then, the reduced basis functions $\{\zeta_l^k(\mathbf{x})\}_{l=1}^{m_k}$ have the following approximation property*

$$\frac{\sum_{q=1}^Q \left\| \tilde{\phi}_k^{\text{loc}}(\mathbf{x}, \omega_q) - \sum_{l=1}^{m_k} (\tilde{\phi}_k^{\text{loc}}(\mathbf{x}, \omega_q), \zeta_l^k(\mathbf{x}))_X \zeta_l^k(\mathbf{x}) \right\|_X^2}{\sum_{q=1}^Q \left\| \tilde{\phi}_k^{\text{loc}}(\mathbf{x}, \omega_q) \right\|_X^2} = \frac{\sum_{s=m_k+1}^Q \lambda_s}{\sum_{s=1}^Q \lambda_s}, \quad (17)$$

where $X = L^2(D)$ or $X = H^1(D)$ and the number m_k is determined according to the ratio $\rho = \frac{\sum_{s=1}^{m_k} \lambda_s}{\sum_{s=1}^Q \lambda_s}$.

In practice, we choose the first m_k dominant reduced basis functions such that ρ is close enough to 1 to achieve a desired accuracy, say $\rho = 99\%$. More details of the POD method can be found in [5, 38]. Notice that reduced basis functions $\zeta_0^k(\mathbf{x})$ and $\zeta_l^k(\mathbf{x})$, $l = 1, \dots, m_k$ approximately capture the mean profile and the fluctuation of multiscale basis functions associated with \mathbf{x}_k , respectively. Thus, it is expected that for each realization of the random potential the associated multiscale basis functions can be approximated by the reduced basis functions, i.e.,

$$\phi_k^{\text{loc}}(\mathbf{x}, \omega) \approx \zeta_0^k(\mathbf{x}) + \sum_{l=1}^{m_k} c_l(\omega) \zeta_l^k(\mathbf{x}). \quad (18)$$

Remark 3.2. To construct the multiscale reduced basis functions, we partition the coarse grids D^k into fine-scale quadrilateral elements with meshsize $h \ll \varepsilon$, which requires additional computational cost in the offline stage. However, the precomputed reduced basis functions can be used repeatedly to solve (1) for each realization of the random potential and different initial data, which results in considerable savings.

3.3. Estimation of the number of learning samples

We shall study the continuous dependence of multiscale basis functions on the random potential, which provide a guidance on how to determine the number of samples in the construction of multiscale basis functions. For notational simplification, we carry out the analysis for multiscale basis functions without localization.

Let $\varphi_s^h(\mathbf{x})$, $s = 1, \dots, N_h$ denote the finite element basis functions defined on fine mesh with size h and N_h is the number of fine-scale finite element basis functions. When we numerically solve (4)-(5), we represent the multiscale basis function as $\phi_i(\mathbf{x}) = \sum_{s=1}^{N_h} c_s \varphi_s^h(\mathbf{x})$ and obtain the following quadratic programming problem with equality constraints

$$\begin{cases} \min_{\mathbf{c}} \frac{1}{2} \mathbf{c}^T Q \mathbf{c}, \\ \text{s.t. } A \mathbf{c} = \mathbf{b}, \end{cases} \quad (19)$$

where $\mathbf{c} = [c_1, \dots, c_{N_h}]^T$ is the coefficients and Q is a symmetric positive definite matrix on the fine triangularization \mathcal{T}_h with the (i, j) component

$$Q_{ij} = \frac{\varepsilon^2}{2} (\nabla \varphi_i^h, \nabla \varphi_j^h) + (v^\varepsilon(\mathbf{x}, \omega_q) \varphi_i^h, \varphi_j^h). \quad (20)$$

In (19), A is an N_h -by- N_H matrix with $A_{ij} = (\varphi_i^h, \varphi_j^H)$ and \mathbf{b} an N_h -by-1 vector with only the i -th entry being 1 and others being 0.

The following result states the continuous dependence of multiscale basis functions on the random potential.

Theorem 3.2. Assume the random potential $v^\varepsilon(\mathbf{x}, \omega)$ is almost surely bounded, i.e. (14) is satisfied and mesh size of the fine-scale triangles is small such that: (1) $h/\varepsilon = \kappa$ is small; and (2) $h^d \|v^\varepsilon(\cdot, \omega_1) - v^\varepsilon(\cdot, \omega_2)\|_{L^\infty(D)} < 1$. Then for two realizations ω_1 and ω_2 of the random potential $v^\varepsilon(\mathbf{x}, \omega)$, the corresponding multiscale basis functions satisfy

$$\|\phi(\cdot, \omega_1) - \phi(\cdot, \omega_2)\|_{L^\infty(D)} \leq \frac{C}{\kappa^6} \varepsilon^{-2} \|v^\varepsilon(\cdot, \omega_1) - v^\varepsilon(\cdot, \omega_2)\|_{L^\infty(D)}, \quad (21)$$

where the constant C is independent of h, ε , and $\|v^\varepsilon(\cdot, \omega_1) - v^\varepsilon(\cdot, \omega_2)\|_{L^\infty(D)}$.

Proof. Under the assumptions that $v^\varepsilon(\mathbf{x}, \omega)$ is almost surely bounded and $h/\varepsilon = \kappa$ is small, we know that Q is a positive definite matrix. Moreover, we know that A has full rank, i.e., $\text{rank}(A) = N_H$. Therefore, the quadratic optimization problem (19) has a unique minimizer, satisfying the Karush-Kuhn-Tucker condition. Specifically, the unique minimizer of (19) can be explicitly written as

$$\mathbf{c} = Q^{-1} A^T (A Q^{-1} A^T)^{-1} \mathbf{b}. \quad (22)$$

For two realizations ω_1 and ω_2 , we define $\delta V = Q_1 - Q_2$. Then

$$(\delta V)_{ij} = ((v(\cdot, \omega_1) - v(\cdot, \omega_2)) \varphi_i^h, \varphi_j^h), \quad (23)$$

and thus

$$\|\delta V\|_\infty \leq h^d \|v^\varepsilon(\cdot, \omega_1) - v^\varepsilon(\cdot, \omega_2)\|_{L^\infty(D)}. \quad (24)$$

We choose h to be small enough such that $\|\delta V\|_\infty \leq 1$, and have

$$Q_2^{-1} = \sum_{n=0}^{\infty} (Q_1^{-1} \delta V)^n Q_1^{-1},$$

and thus

$$\begin{aligned} \mathbf{c}_2 - \mathbf{c}_1 &= [Q_2^{-1} - Q_1^{-1}] A^T (A Q_1^{-1} A^T)^{-1} \mathbf{b} + Q_2^{-1} A^T [(A Q_2^{-1} A^T)^{-1} - (A Q_1^{-1} A^T)^{-1}] \mathbf{b}, \\ &= Q_1^{-1} \delta V Q_1^{-1} A^T (A Q_1^{-1} A^T)^{-1} \mathbf{b} \\ &\quad - Q_2^{-1} A^T (A Q_1^{-1} A^T)^{-1} (A Q_1^{-1} \delta V Q_1^{-1} A^T) (A Q_1^{-1} A^T)^{-1} \mathbf{b} + o(\|\delta V\|_\infty), \\ &= Q_1^{-1} \delta V Q_1^{-1} A^T (A Q_1^{-1} A^T)^{-1} \mathbf{b} \\ &\quad - Q_1^{-1} A^T (A Q_1^{-1} A^T)^{-1} (A Q_1^{-1} \delta V Q_1^{-1} A^T) (A Q_1^{-1} A^T)^{-1} \mathbf{b} + o(\|\delta V\|_\infty). \end{aligned}$$

Therefore,

$$|\mathbf{c}_2 - \mathbf{c}_1|_\infty \leq C \|A\|_\infty \|Q_1^{-1}\|_\infty^2 \|(A Q_1^{-1} A^T)^{-1}\|_\infty |\mathbf{b}|_\infty (1 + \|A\|_\infty^2 \|Q_1^{-1}\|_\infty \|(A Q_1^{-1} A^T)^{-1}\|_\infty) \|\delta V\|_\infty.$$

By their definitions, we have

$$\|A\|_\infty \leq C h^d, \quad |\mathbf{b}|_\infty = 1, \quad \|Q_1^{-1}\|_\infty \leq C h^{-2}, \quad \|Q_1\|_\infty \leq C \max\{\varepsilon^2, h^2\} \leq C \varepsilon^2,$$

and thus

$$|\mathbf{c}_2 - \mathbf{c}_1|_\infty \leq C \varepsilon^4 h^{-6} h^{-d} \|\delta V\|_\infty \leq C \varepsilon^4 h^{-6} \|v^\varepsilon(\cdot, \omega_2) - v^\varepsilon(\cdot, \omega_1)\|_{L^\infty(D)}.$$

We complete the proof since $h/\varepsilon = \kappa$ and $\|\phi(\cdot, \omega_2) - \phi(\cdot, \omega_1)\|_{L^\infty(D)} \leq |\mathbf{c}_2 - \mathbf{c}_1|_\infty$. \square

Equipped with **Theorem 3.2**, we can estimate the number of samples in the construction of multiscale reduced basis functions. Suppose the random potential is of the form (16). For any $\delta > 0$, we choose an integer Q_δ and a set of random samples $\{v^\varepsilon(\mathbf{x}, \omega_q)\}_{q=1}^{Q_\delta}$ such that

$$\mathbb{E} \left[\inf_{1 \leq q \leq Q_\delta} \|v_m^\varepsilon(\mathbf{x}, \omega) - v_m^\varepsilon(\mathbf{x}, \omega_q)\|_{L^\infty(D)} \right] \leq \delta, \quad (25)$$

where the expectation is taken over the random variables in $v_m^\varepsilon(\mathbf{x}, \omega)$ of the form (16). We can give a way to choose the random samples $\{v^\varepsilon(\mathbf{x}, \omega_q)\}_{q=1}^{Q_\delta}$ since the distribution of the random variables $\xi_i(\omega)$, $i = 1, \dots, m$ is known.

For every $\mathbf{x}_k \in \mathcal{N}$, let $\{\phi_k(\mathbf{x}, \omega_q)\}_{q=1}^{Q_\delta}$ be the samples of multiscale basis functions associated with \mathbf{x}_k . Then, we have

$$\mathbb{E} \left[\inf_{1 \leq q \leq Q_\delta} \|\phi_k(\mathbf{x}, \omega) - \phi_k(\mathbf{x}, \omega_q)\|_{L^\infty(D)} \right] \leq \frac{C}{\kappa^6} \varepsilon^{-2} \delta. \quad (26)$$

Given parameters ε and h , we choose δ and Q_δ so that the right-hand side of (26) is small. Then the space of multiscale basis functions can be well approximated by the samples of multiscale basis functions $\{\phi_k(\mathbf{x}, \omega_q)\}_{q=1}^{Q_\delta}$ with controllable accuracy and the POD method is further applied to construct multiscale reduced basis functions.

3.4. Derivation of our method based on the multiscale reduced basis functions

In this section, we present our method for solving the random Schrödinger equation: in the physical space, we use the multiscale reduced basis functions obtained in §3.2; in the random space, we use the qMC method.

The implementation of the qMC method is fairly easy. For instance, given a set of qMC samples, expectation of the solution is approximated by

$$\mathbb{E} [\psi^\varepsilon(t, \mathbf{x}, \omega)] \approx \frac{1}{n} \sum_{i=1}^n \psi^\varepsilon(t, \mathbf{x}, \omega_i), \quad (27)$$

where n is the number of qMC samples. Details of the generation of qMC samples and its convergence analysis will be discussed in §4.

Now, we focus on how to approximate the wavefunction in the physical space for each qMC sample ω_s . For each node point $\mathbf{x}_k \in \mathcal{N}$, we have constructed a set of multiscale reduced basis functions $\{\zeta_i^k\}_{i=0}^{m_k}$ and represent the wavefunction by

$$\psi^\varepsilon(t, \mathbf{x}, \omega_s) = \sum_{k=1}^{N_H} \sum_{l=0}^{m_k} c_l^k(t, \omega_s) \zeta_l^k(\mathbf{x}), \quad (28)$$

where m_k is the number of multiscale reduced basis functions associated with the node \mathbf{x}_k . In the Galerkin formulation, we have the following weak form

$$\left(i\varepsilon \partial_t \sum_{k=1}^{N_H} \sum_{l=0}^{m_k} c_l^k(t, \omega_s) \zeta_l^k(\mathbf{x}), \zeta_r^j(\mathbf{x}) \right) = \left(\mathcal{H}(\mathbf{x}, \omega_s) \sum_{k=1}^{N_H} \sum_{l=0}^{m_k} c_l^k(t, \omega_s) \zeta_l^k(\mathbf{x}), \zeta_r^j(\mathbf{x}) \right), \quad (29)$$

$\mathbf{x} \in D, \quad t \in \mathbb{R}, \quad j = 1, \dots, N_H, \quad r = 0, \dots, m_k,$

where $\mathcal{H}(\mathbf{x}, \omega_s)$ is a deterministic operator. To numerically solve (29), we introduce some notations. Let S , M , and $V(\omega_s)$ be matrices with dimension $\sum_{k=1}^{N_H} (m_k + 1) \times \sum_{k=1}^{N_H} (m_k + 1)$. Their entries are given by

$$\begin{aligned} S_{\sum_{i=1}^k (m_i+1)+l, \sum_{i=1}^j (m_i+1)+r} &= \int_D \nabla \zeta_l^k \cdot \nabla \zeta_r^j d\mathbf{x}, \\ M_{\sum_{i=1}^k (m_i+1)+l, \sum_{i=1}^j (m_i+1)+r} &= \int_D \zeta_l^k \zeta_r^j d\mathbf{x}, \\ V_{\sum_{i=1}^k (m_i+1)+l, \sum_{i=1}^j (m_i+1)+r}(\omega_s) &= \int_D \zeta_l^k v^\varepsilon(\mathbf{x}, \omega_s) \zeta_r^j d\mathbf{x}. \end{aligned}$$

Then, we can reduce the weak formulation (29) into the following ODE system

$$i\varepsilon M \frac{d\mathbf{c}(t, \omega_s)}{dt} = \left(\frac{\varepsilon^2}{2} S + V(\omega_s) \right) \mathbf{c}(t, \omega_s), \quad (30)$$

where the column vector $\mathbf{c}(t, \omega_s) = (c_0^1(t, \omega_s), \dots, c_{m_k}^1(t, \omega_s), \dots, c_0^{N_H}(t, \omega_s), \dots, c_{m_k}^{N_H}(t, \omega_s))^T$ consisting of all expansion coefficients of the solution $\psi^\varepsilon(t, \mathbf{x}, \omega_s)$ onto multiscale reduced basis functions. We can further rewrite (30) as

$$\frac{d\mathbf{c}(t, \omega_s)}{dt} = \frac{1}{i\varepsilon} B(\omega_s) \mathbf{c}(t, \omega_s) \quad (31)$$

where $B(\omega_s) = M^{-1}A(\omega_s)$ and $A(\omega_s) = \frac{\varepsilon^2}{2}S + V(\omega_s)$. In the end, we can solve the above ODE system using existing ODE solvers.

Before ending this section, we shall explain why we choose the qMC method to approximate the random space of the electron wavefunction. Since the parameterization of a random potential may have high dimension, i.e., m is large in (15), non-intrusive methods, such as sparse grid method [6] and stochastic collocation method [33], become prohibitively expensive to solve PDEs with random coefficients. Polynomial chaos expansion (PCE) methods [19, 41] are also frequently used in the literature to solve PDEs with random coefficients. This type of methods is useful if the solution is sufficiently smooth in the random space with small dimensionality. The performance of MC method does not depend on the dimension of the random space. However, its convergence rate is merely $O(\frac{1}{\sqrt{n}})$. The convergence rate of the qMC method is better both theoretically and numerically; see (45) in Theorem 4.5. Therefore, we choose the qMC method and its implementation is almost the same as the MC method.

4. Convergence analysis

We shall analyze the approximation error of the proposed method, where the emphasis is put on computing functionals of the wavefunction.

4.1. Regularity of the wavefunction with respect to the random variables

Since the potential $v^\varepsilon(\mathbf{x}, \omega)$ in (1) is parametrized by m random variables $\xi_i(\omega)$, $i = 1, \dots, m$ in (16), i.e., $v_m^\varepsilon(\mathbf{x}, \omega) = v^\varepsilon(\mathbf{x}, \xi_1(\omega), \dots, \xi_m(\omega))$. The wavefunction $\psi_m^\varepsilon(t, \mathbf{x}, \omega)$ satisfies

$$\begin{cases} i\varepsilon\partial_t\psi_m^\varepsilon = -\frac{\varepsilon^2}{2}\Delta\psi_m^\varepsilon + v_m^\varepsilon(\mathbf{x}, \omega)\psi_m^\varepsilon, & \mathbf{x} \in D, \quad t \in \mathbb{R}, \\ \psi_m^\varepsilon \in H_P^1(D), \\ \psi_m^\varepsilon|_{t=0} = \psi_{\text{in}}(\mathbf{x}). \end{cases} \quad (32)$$

The Doob-Dynkin's lemma implies the wavefunction $\psi_m^\varepsilon(t, \mathbf{x}, \omega)$ in (32) can also be represented by a functional of these random variables, i.e., $\psi^\varepsilon(t, \mathbf{x}, \omega) = \psi^\varepsilon(t, \mathbf{x}, \xi_1(\omega), \dots, \xi_m(\omega))$.

First of all, we analyze the error introduced by the parameterization of the random potential. We have the following estimate result.

Lemma 4.1. *The difference between wavefunctions to (32) and (1) satisfies*

$$\|\psi_m^\varepsilon - \psi^\varepsilon\|_{L^2(\Omega, D)} \leq \frac{T}{\varepsilon} \|v_m^\varepsilon - v^\varepsilon\|_{L^\infty(\Omega, D)}, \quad \forall t \in [0, T]. \quad (33)$$

Proof. The difference $\delta\psi = \psi_m^\varepsilon - \psi^\varepsilon$ satisfies

$$\begin{cases} i\varepsilon\partial_t\delta\psi = -\frac{\varepsilon^2}{2}\Delta\delta\psi + v_m^\varepsilon\delta\psi + (v_m^\varepsilon - v^\varepsilon)\psi^\varepsilon, & \mathbf{x} \in D, \quad t \in \mathbb{R}, \\ \delta\psi \in H_P^1(D), \\ \delta\psi|_{t=0} = 0. \end{cases}$$

By a direct calculation, we have

$$\frac{d}{dt} \|\delta\psi\|_{L^2(\Omega, D)}^2 = \frac{1}{i\varepsilon} \int_{\Omega} \int_D (\overline{\delta\psi}(v_m^\varepsilon - v^\varepsilon)\psi^\varepsilon - \overline{\psi^\varepsilon}(v_m^\varepsilon - v^\varepsilon)\delta\psi) \, d\mathbf{x}d\rho(\omega),$$

where $\rho(\omega)$ is the probability measure induced by the randomness in the potential (16) and thus

$$\begin{aligned} \frac{d}{dt} \|\delta\psi\|_{L^2(\Omega, D)}^2 &\leq \frac{2}{\varepsilon} \int_{\Omega} \int_D |\overline{\delta\psi}(v_m^\varepsilon - v^\varepsilon)\psi^\varepsilon| \, d\mathbf{x}d\rho(\omega) \leq \frac{2}{\varepsilon} \int_{\Omega} \|\overline{\delta\psi}\|_{L^2(D)} \|v_m^\varepsilon - v^\varepsilon\|_{L^2(D)} \, d\rho(\omega), \\ &\leq \frac{2}{\varepsilon} \int_{\Omega} \|\delta\psi\|_{L^2(D)} \|v_m^\varepsilon - v^\varepsilon\|_{L^\infty(D)} \, d\rho(\omega) \leq \frac{2\|v_m^\varepsilon - v^\varepsilon\|_{L^\infty(D, \Omega)}}{\varepsilon} \|\delta\psi\|_{L^2(D, \Omega)}. \end{aligned}$$

Therefore, we obtain

$$\|\delta\psi\|_{L^2(\Omega, D)} \leq \frac{T}{\varepsilon} \|v_m^\varepsilon - v^\varepsilon\|_{L^\infty(\Omega, D)}, \quad \forall t \in [0, T],$$

which completes the proof. \square

To analyze the qMC method, it is crucial to bound the mixed first derivatives of ψ_m^ε with respect to $\xi_i(\omega)$. Denote $\boldsymbol{\xi}(\omega) = (\xi_1(\omega), \dots, \xi_m(\omega))^T$ for convenience. Let $\boldsymbol{\nu} = (\nu_1, \dots, \nu_m)$ denote a multi-index of non-negative integers, with $|\boldsymbol{\nu}| = \sum_{j=1}^m \nu_j$ and $|\boldsymbol{\nu}|_\infty = \max_{1 \leq j \leq m} \nu_j$. The value of ν_j determines the number of derivatives to be taken with respect to ξ_j , and $\partial^{\boldsymbol{\nu}}\psi_m^\varepsilon$ denotes the mixed derivative of ψ_m^ε with respect to all variables specified by the multi-index $\boldsymbol{\nu}$.

Lemma 4.2. For any $\omega \in \Omega$, any time T , and for any multi-index $\boldsymbol{\nu}$ with $|\boldsymbol{\nu}| < \infty$, the partial derivative of $\psi_m^\varepsilon(t, \mathbf{x}, \omega)$ satisfies the following a-priori estimate

$$\|\partial^\nu \psi_m^\varepsilon(t, \cdot, \omega)\|_{L^2(D)} \leq \frac{|\boldsymbol{\nu}|! T^{|\boldsymbol{\nu}|}}{\varepsilon^{|\boldsymbol{\nu}|}} \left\{ \prod_{j \geq 1} \left(\sqrt{\lambda_j} \|v_j\|_{C^0(\bar{D})} \right)^{\nu_j} \right\}, \quad \forall t \in [0, T]. \quad (34)$$

Proof. When $|\boldsymbol{\nu}| = 1$, we take the derivative of (32) with respect to $\xi_j(\omega)$. Let $\partial_j \psi_m = \partial_{\xi_j} \psi_m^\varepsilon$ and $\partial_j v_m = \partial_{\xi_j} v_m^\varepsilon$, we have

$$i\varepsilon (\partial_j \psi_m)_t = -\frac{\varepsilon^2}{2} \Delta (\partial_j \psi_m) + (\partial_j v_m) \psi_m^\varepsilon + v_m^\varepsilon (\partial_j \psi_m).$$

Thereafter, we have the following estimate by a direction calculation

$$\begin{aligned} \frac{d}{dt} \|\partial_j \psi_m\|_{L^2(D)}^2 &= \int_D \{ (\overline{\partial_j \psi_m})_t (\partial_j \psi_m) + (\overline{\partial_j \psi_m}) (\partial_j \psi_m)_t \} d\mathbf{x}, \\ &= \int_D \left(-\frac{1}{i\varepsilon} (\partial_j v_m) \overline{\psi_m^\varepsilon} (\partial_j \psi_m) + \frac{1}{i\varepsilon} (\overline{\partial_j \psi_m}) (\partial_j v) \psi_m^\varepsilon \right) d\mathbf{x}, \\ &\leq \frac{2}{\varepsilon} \|\partial_j \psi_m\|_{L^2(D)} \|\partial_j v \psi_m^\varepsilon\|_{L^2(D)} \leq \frac{2}{\varepsilon} \|\partial_j \psi_m\|_{L^2(D)} \|\partial_j v_m\|_{L^\infty(D)}, \end{aligned}$$

and

$$\|\partial_j \psi_m\|_{L^2(D)} \leq \frac{T}{\varepsilon} \|\partial_j v_m\|_{L^\infty(D)} \leq \frac{T}{\varepsilon} \sqrt{\lambda_j} \|\phi_j\|_{C^0(\bar{D})}. \quad (35)$$

When $|\boldsymbol{\nu}| \geq 2$, we have

$$i\varepsilon (\partial^\nu \psi_m)_t = -\frac{\varepsilon^2}{2} \Delta (\partial^\nu \psi_m) + \sum_{\substack{\boldsymbol{\mu} \leq \boldsymbol{\nu} \\ \boldsymbol{\mu} \neq \boldsymbol{\nu}}} \binom{\boldsymbol{\nu}}{\boldsymbol{\mu}} (\partial^{\boldsymbol{\nu}-\boldsymbol{\mu}} v_m) (\partial^\mu \psi_m) + v_m^\varepsilon (\partial^\nu \psi_m).$$

According to the definition of the random potential (15), we have $\partial^{\boldsymbol{\nu}-\boldsymbol{\mu}} v_m^\varepsilon = 0$ if $|\boldsymbol{\nu} - \boldsymbol{\mu}| \geq 2$. Thus the above equation can be simplified as

$$i\varepsilon (\partial^\nu \psi_m)_t = -\frac{\varepsilon^2}{2} \Delta (\partial^\nu \psi_m) + \sum_{|\boldsymbol{\nu}-\boldsymbol{\mu}|=1} \binom{|\boldsymbol{\nu}|}{1} (\partial^{\boldsymbol{\nu}-\boldsymbol{\mu}} v_m) (\partial^\mu \psi_m) + v_m^\varepsilon (\partial^\nu \psi_m).$$

Similarly, we obtain

$$\begin{aligned} \frac{d}{dt} \|\partial^\nu \psi_m\|_{L^2(D)}^2 &= \int_D \{ (\overline{\partial^\nu \psi_m})_t (\partial^\nu \psi_m) + (\overline{\partial^\nu \psi_m}) (\partial^\nu \psi_m)_t \} d\mathbf{x}, \\ &= \sum_{|\boldsymbol{\nu}-\boldsymbol{\mu}|=1} \binom{|\boldsymbol{\nu}|}{1} \int_D \left(-\frac{1}{i\varepsilon} (\partial^{\boldsymbol{\nu}-\boldsymbol{\mu}} v_m) \overline{(\partial^\mu \psi_m)} (\partial^\nu \psi_m) + \frac{1}{i\varepsilon} (\overline{\partial^\nu \psi_m}) (\partial^{\boldsymbol{\nu}-\boldsymbol{\mu}} v_m) (\partial^\mu \psi_m) \right) d\mathbf{x}, \\ &\leq \frac{2|\boldsymbol{\nu}|}{\varepsilon} \|\partial^\nu \psi_m\|_{L^2(D)} \sum_{|\boldsymbol{\nu}-\boldsymbol{\mu}|=1} \|(\partial^{\boldsymbol{\nu}-\boldsymbol{\mu}} v_m)\|_{L^\infty(D)} \|(\partial^\mu \psi_m)\|_{L^2(D)}, \end{aligned}$$

and

$$\|\partial^\nu \psi_m\|_{L^2(D)} \leq \frac{T^{|\nu|}}{\varepsilon} \sum_{|\nu-\mu|=1} \|(\partial^{\nu-\mu} v_m)\|_{L^\infty(D)} \|(\partial^\mu \psi_m)\|_{L^2(D)}. \quad (36)$$

Now we are ready to prove the theorem by mathematical induction. From (35), we know that (34) holds for $|\nu| = 1$. Assume that (34) holds for μ with $|\nu - \mu| = 1$. Substituting this into (36) yields the desired estimate for the ν case. \square

Remark 4.1. The above derivation is similar to that in [25], where an estimate in $L^2(D, \Omega)$ norm is obtained. Here, for each random realization ω , we have the estimate (34) in $L^2(D)$ norm, which will be used to prove the convergence in qMC.

4.2. Main result of the error analysis

In the framework of uncertainty quantification, we are interested in computing some statistical quantities of the electron wavefunction. As such, we shall present the error analysis of our method in computing functionals of ψ_m^ε .

Let $\mathcal{G}(\cdot)$ be a continuous linear functional on $L^2(D)$, then there exists a constant $C_{\mathcal{G}}$ such that

$$|\mathcal{G}(u)| \leq C_{\mathcal{G}} \|u\|_{L^2(D)},$$

for all $u \in L^2(D)$. Consider the following integral

$$I_m(F) = \int_{\xi \in [0,1]^m} F(\xi) d\xi \quad (37)$$

with $F(\xi) = \mathcal{G}(\psi_m^\varepsilon(\cdot, \xi))$. We approximate the integral over the unit cube by randomly shifted lattice rules

$$Q_{m,n}(\Delta; F) \triangleq \frac{1}{n} \sum_{i=1}^n F\left(\text{frac}\left(\frac{i\mathbf{z}}{n} + \Delta\right)\right),$$

where $\mathbf{z} \in \mathbb{N}^m$ is the (deterministic) generating vector and $\Delta \in [0,1]^m$ is the random shift which is uniformly distributed over $[0,1]^m$. Notice that m is the dimension of the random vector ξ in the random potential and n is the number of the sample point in implementing the qMC method. The interested reader is referred to [11] for more details of the randomly shifted lattice rules in the qMC method.

Lemma 4.3. *Let F be the integrand in (37). Given $m, n \in \mathbb{N}$ with $n \leq 10^{30}$, weights $\gamma = (\gamma_{\mathbf{u}})_{\mathbf{u} \in \mathbb{N}}$, a randomly shifted lattice rule with n points in m dimensions can be constructed by a component-by-component algorithm such that, for all $\lambda \in (1/2, 1]$,*

$$\sqrt{\mathbb{E}^\Delta |I_m(F) - Q_{m,n}(\cdot; F)|^2} \leq 9C^* C_{\gamma,m}(\lambda) n^{-1/(2\lambda)}, \quad (38)$$

with

$$C_{\gamma,m}(\lambda) = \left(\sum_{\emptyset \neq \mathbf{u} \subseteq \{1:m\}} \gamma_{\mathbf{u}}^\lambda \prod_{j \in \mathbf{u}} \varrho(\lambda) \right)^{1/(2\lambda)} \left(\sum_{\mathbf{u} \subseteq \{1:m\}} \frac{(|\mathbf{u}|!)^2 T^{2|\mathbf{u}|}}{\gamma_{\mathbf{u}} \varepsilon^{2|\mathbf{u}|}} \prod_{j \in \mathbf{u}} \lambda_j \|\phi_j\|_{C^0(\bar{D})}^2 \right)^{1/2}. \quad (39)$$

Proof. The proof of this result is essentially an application of the Koksma-Hlawka inequality, which is the same as the proofs of Theorem 15, Theorem 16, and Theorem 17 in [20], or Theorem 5.10 in [11] with the following modification of estimates:

$$\varrho(\lambda) = 2 \left(\frac{\sqrt{2\pi}}{\pi^{2-2\eta_*}(1-\eta_*)\eta_*} \right)^\lambda \zeta\left(\lambda + \frac{1}{2}\right), \quad \eta_* = \frac{2\lambda - 1}{4\lambda} \quad (40)$$

with $\zeta(x) = \sum_{j=1}^{\infty} j^{-x}$ the Riemann zeta function, and $C^* = \|\mathcal{G}\|_{L^2(D)}$. \square

To analyze the error of our method, we need to make some assumptions on the regularity of the eigenfunctions and the decay rate of the eigenvalues in the KL expansion (16) of the random potential.

Assumption 4.4. (a) *There exist $C > 0$ and $\Theta > 1$ such that $\lambda_j \leq Cj^{-\Theta}$ for $j \geq 1$;*

(b) *The Karhunen-Loève eigenfunctions $v_j(\mathbf{x})$ are continuous and there exist $C > 0$ and $\eta \in [0, \frac{\Theta-1}{2\Theta})$ such that $\|v_j\|_{C^0(\bar{D})} \leq C\lambda_j^{-\eta}$ for $j \geq 1$;*

(c) *The sequence defined by $\sqrt{\lambda_j}\|v_j\|_{C^0(\bar{D})}$, $j \geq 1$ satisfies $\sum_{j \geq 1} (\sqrt{\lambda_j}\|v_j\|_{C^0(\bar{D})})^p < \infty$ for some $p \in (0, 1]$, and $\sum_{j \geq 1} \sqrt{\lambda_j}\|v_j\|_{C^0(\bar{D})} < \frac{\varepsilon}{T} \sqrt{\varrho(\lambda)}$ for $\lambda \in (1/2, 1]$.*

Recall that ψ^ε and ψ_m^ε are solutions to (1) and (32), respectively. Denote $\psi_{H,m}^\varepsilon$ the solution obtained by our method using the multiscale reduced basis functions in the physical space and the qMC method in the random space. Under the assumptions for the random potential, we have the error estimate.

Theorem 4.5. *Consider the approximation of $\mathbb{E}[\mathcal{G}(\psi^\varepsilon)]$ via qMC multiscale finite element methods, denoted by $Q_{m,n}(\cdot; \mathcal{G}(\psi_{H,m}^\varepsilon))$, where we assume $\psi^\varepsilon \in L^2(\Omega; H^2(D))$. A randomly shifted lattice rule $Q_{m,n}$ is applied to $\mathcal{G}(\psi_m^\varepsilon)$. Then, we can bound the root-mean-square error with respect to the uniformly distributed shift $\Delta \in [0, 1]^m$ by*

$$\sqrt{\mathbb{E}^\Delta \left[\left(\mathbb{E}[\mathcal{G}(\psi^\varepsilon)] - Q_{m,n}(\cdot; \mathcal{G}(\psi_{H,m}^\varepsilon)) \right)^2 \right]} \leq C \left(\frac{H^2}{\varepsilon^2} + \frac{m^{-\chi}}{\varepsilon} + n^{-r} \right), \quad 0 < t \leq T, \quad (41)$$

for $0 < \chi \leq (1/2 - \eta)\Theta - 1/2$, and with $r = 1/p - 1/2$ for $p \in (2/3, 1]$ and $r = 1 - \delta$ for $p \leq 2/3$, with δ arbitrarily small. Here the constant C is independent of ε , m , and n but depends on T .

Proof. The linearity of operator \mathcal{G} implies

$$\mathcal{G}(\psi^\varepsilon) - \mathcal{G}(\psi_{H,m}^\varepsilon) = \mathcal{G}(\psi^\varepsilon) - \mathcal{G}(\psi_H^\varepsilon) + \mathcal{G}(\psi_H^\varepsilon) - \mathcal{G}(\psi_{H,m}^\varepsilon). \quad (42)$$

Under the assumption $\psi^\varepsilon \in L^2(\Omega; H^2(D))$, we have, see for example [7],

$$|\mathbb{E}[\mathcal{G}(\psi^\varepsilon) - \mathcal{G}(\psi_H^\varepsilon)]| \leq C \frac{H^2}{\varepsilon^2}. \quad (43)$$

Under the assumptions (b) and (c) in Assumption 4.4, we have, based on Lemma 4.1,

$$|\mathcal{G}(\psi_H^\varepsilon) - \mathcal{G}(\psi_{H,m}^\varepsilon)| \leq C \frac{m^{-\chi}}{\varepsilon} \quad (44)$$

for all $0 < \chi \leq (1/2 - \eta)\Theta - 1/2$. Detailed derivation is essentially the same as the proof of Theorem 8 in [20].

Finally, when applying the qMC method to (42), we need to analyze the error in the qMC method. We adopt the standard framework, i.e., the Koksma-Hlawka inequality. Under **Assumption 4.4**, we have, based on Lemma 4.2 and Lemma 4.3,

$$\sqrt{\mathbb{E}^\Delta |I_m(F) - Q_{m,n}(\cdot; F)|^2} \leq Cn^{-r}, \quad (45)$$

where $r = 1/p - 1/2$ for $p \in (2/3, 1]$ and $r = 1 - \delta$ for $p \leq 2/3$, with δ arbitrarily small. Detailed derivation is essentially the same as the proof of Theorem 20 in [20]. A combination of above estimates completes the proof. \square

Remark 4.2. The term $\frac{m^{-\chi}}{\varepsilon}$ in the error estimate (41) can be viewed as a modeling error. When the m -term KL truncation potential $v_m^\varepsilon(\mathbf{x}, \omega)$ in (16) provides an accurate approximation to the potential $v^\varepsilon(\mathbf{x}, \omega)$, the term $\frac{m^{-\chi}}{\varepsilon}$ becomes small or negligible.

Remark 4.3. In §5, we will show the proposed method works well for a large class of random potentials, even when the eigenvalues in the KL expansion have a relatively slow decay rate. Therefore, **Assumption 4.4** is a rather technical assumption for the convergence analysis of the proposed method.

Remark 4.4. In the error analysis for the qMC method, we assume $\boldsymbol{\xi} = (\xi_1, \dots, \xi_m) \in [0, 1]^m$ for notational convenience; see (37), where ξ_i are i.i.d. uniform random variables. In the KL expansion (16) representation for $v_m^\varepsilon(\mathbf{x}, \omega)$, we choose $\xi_i \in [-\sqrt{3}, \sqrt{3}]$, $i = 1, \dots, m$ so that the conditions $\mathbb{E}[\xi_i] = 0$, $\mathbb{E}[\xi_i \xi_j] = \delta_{ij}$ are satisfied. The same convergence result can be obtained with little modification of the current proof.

5. Numerical examples

In this section, we conduct numerical experiments to test the accuracy and the efficiency of our method. Specifically, we will present convergence tests with respect to the physical meshsize, the number of multiscale reduced basis functions, and the number of qMC samples. In addition, we will investigate the existence of Anderson localization in both 1D and 2D. For convenience, we first introduce L^2 norm and H^1 norm as

$$\|\psi^\varepsilon\|_{L^2}^2 = \int_D |\psi^\varepsilon|^2 d\mathbf{x}, \quad \|\psi^\varepsilon\|_{H^1}^2 = \int_D |\nabla \psi^\varepsilon|^2 d\mathbf{x} + \int_D |\psi^\varepsilon|^2 d\mathbf{x}.$$

In what follows, we compare the relative error between expectations of the numerical solution $\psi_{\text{num}}^\varepsilon$ and the reference solution $\psi_{\text{ref}}^\varepsilon$ in both L^2 norm and H^1 norm

$$\begin{aligned} \text{Error}_{L^2} &= \frac{\|\mathbb{E}[\psi_{\text{num}}^\varepsilon] - \mathbb{E}[\psi_{\text{ref}}^\varepsilon]\|_{L^2}}{\|\mathbb{E}[\psi_{\text{ref}}^\varepsilon]\|_{L^2}}, \\ \text{Error}_{H^1} &= \frac{\|\mathbb{E}[\psi_{\text{num}}^\varepsilon] - \mathbb{E}[\psi_{\text{ref}}^\varepsilon]\|_{H^1}}{\|\mathbb{E}[\psi_{\text{ref}}^\varepsilon]\|_{H^1}}. \end{aligned}$$

Here $\mathbb{E}[\psi_{\text{num}}^\varepsilon] = \int_{\Omega} \psi_{\text{num}}^\varepsilon(t, \mathbf{x}, \omega) d\rho(\omega)$, $\mathbb{E}[\psi_{\text{ref}}^\varepsilon] = \int_{\Omega} \psi_{\text{ref}}^\varepsilon(t, \mathbf{x}, \omega) d\rho(\omega)$, Ω is the random space, and $\rho(\omega)$ is the probability measure induced by the randomness in (16). The reference solution refers to the numerical wavefunction using a very fine mesh and a large amount of qMC samples. In numerical experiments, we use the MATLAB's Statistics Toolbox to generate the Sobol sequence to implement the qMC method. When we use the POD method to construct multiscale reduced basis functions, we observed similar decay behaviors of the associated eigenvalues at each coarse grid point. Therefore, we choose the same reduced basis number m_k for all the coarse grid points.

5.1. Convergence in the physical space

Consider the 1D Schrödinger equation over $D = [-\pi, \pi]$

$$i\varepsilon\partial_t\psi^\varepsilon = -\frac{\varepsilon^2}{2}\partial_{xx}\psi^\varepsilon + v^\varepsilon(x, \omega)\psi^\varepsilon, \quad (46)$$

where the periodic condition is imposed, the initial data $\psi_{\text{in}}(x) = (\frac{10}{\pi})^{1/4}e^{-20(x-0)^2}$, and the random potential $v^\varepsilon(x, \omega)$ is defined as

$$v^\varepsilon(x, \omega) = 1 + \sigma \sum_{j=1}^3 \sin(jx^2) \sin(\frac{x}{E_j}) \xi_j(\omega). \quad (47)$$

In the random potential (47), σ is used to control the strength of the random potential, and $\xi_j(\omega)$'s are mean-zero and independent random variables uniformly distributed in $[-\sqrt{3}, \sqrt{3}]$. Moreover, we choose $\varepsilon = \frac{1}{16}$, $\sigma = 1$ and $E = [\frac{1}{9}, \frac{1}{13}, \frac{1}{11}]$, i.e., the characteristic length scale of randomness is different from the semiclassical parameter.

Convergence with respect to the coarse mesh size H . In our numerical test, we set the final computational time $T = 1$. For the reference solution, we choose the fine mesh to be $h = \frac{2\pi}{2048}$ and the qMC sample number to be $n = 16000$. For our method, we choose the POD modes $m_k = 3$, the sampling number in the offline training stage to be 200 and the number of qMC samples in the online stage to be 2560.

In Table 1, we compute the relative errors of the expectation of the wavefunction in both L^2 norm and H^1 norm for a series of coarse meshes with meshsize ranging from $H = \frac{2\pi}{32}$ to $H = \frac{2\pi}{256}$. Nice convergence in the physical space is observed.

H	Error $_{L^2}$	Order	Error $_{H^1}$	Order
$2\pi/32$	0.09862312		0.32096262	
$2\pi/64$	0.00129644	6.25	0.01449534	4.47
$2\pi/128$	0.00002892	5.49	0.00076150	4.25
$2\pi/256$	0.00000950	1.61	0.00014161	2.42

Table 1: Relative L^2 and H^1 errors for the expectation of the wavefunction when $\varepsilon = 1/16$.

Verification of the exponential decay of multiscale basis functions. For the same problem as above, we choose four different realizations of the multiscale basis functions centered

at $x = 0$, i.e. $\phi(x, \boldsymbol{\xi}(\omega_i))$, $i = 1, 2, 3, 4$, which are generated in the offline training stage of our previous experiment when $H = \frac{2\pi}{256}$. In Figure 1a, we plot $\|\nabla\phi(x, \boldsymbol{\xi}(\omega_i))\|_{L_2(D)} / \|\nabla\phi(x, \boldsymbol{\xi}(\omega_i))\|_{L_2(D)}$, $i = 1, 2, 3, 4$. In Figure 1b, we plot the quantity $E_{\text{relative}} = \frac{\|\nabla\phi(x, \boldsymbol{\xi}(\omega_i))\|_{L_2(D)} - \|\nabla\phi(x, \boldsymbol{\xi}(\omega_i))\|_{L_2(D_\ell)}}{\max(\|\nabla\phi(x, \boldsymbol{\xi}(\omega_i))\|_{L_2(D)} - \|\nabla\phi(x, \boldsymbol{\xi}(\omega_i))\|_{L_2(D_\ell)})}$ with respect to the patch size ℓ , which shows the decay rate of E_{relative} with respect to ℓ .

One can see that each realization of the multiscale basis functions decays exponentially fast away from the center $x = 0$. Since the multiscale basis functions have exponential decay property, the approximated multiscale basis using the reduced basis functions (see (18)) still has the same property.

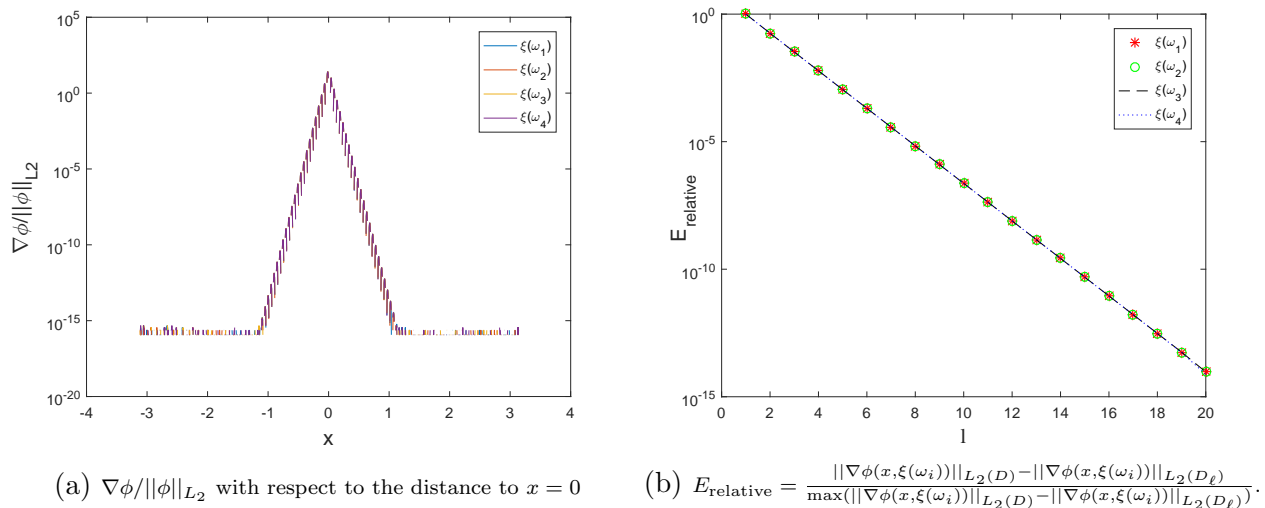


Figure 1: Exponentially decaying properties of the multiscale basis functions for four different realizations.

Convergence with respect to the number of multiscale reduced basis functions.

We study how the approximation error depends on the number of multiscale reduced basis used at each coarse mesh node \mathbf{x}_k , i.e., changing the POD modes m_k . Again, we solve (46) - (47) when $\varepsilon = \frac{1}{16}$, $\sigma = 1$ and $E = [\frac{1}{9}, \frac{1}{13}, \frac{1}{11}]$. The final computational time $T = 1$. For the reference solution, we choose the meshsize to be $h = \frac{2\pi}{2048}$ and the number of qMC samples to be $n = 16000$. For our method, we choose the number of samples in the offline training stage to be 200 and the number of qMC samples in the online stage to be 2560. We fix the coarse mesh size $H = \frac{2\pi}{128}$ and record the relative errors as a function of the number of multiscale reduced basis functions.

In Figure 2, we plot the relative L^2 and H^1 errors with respect to the number of multiscale reduced basis functions. It is observed that results when $m_k = 2$ or $m_k = 3$ have already been good enough in the sense that relative errors are less than 1%. These numerical results indicate that multiscale reduced basis functions can efficiently approximate the physical space of the wavefunction.

5.2. Convergence in the random space

Again, we use the same example: (46) - (47) and $D = [-\pi, \pi]$, but we shall focus on the convergence of our method in random space.

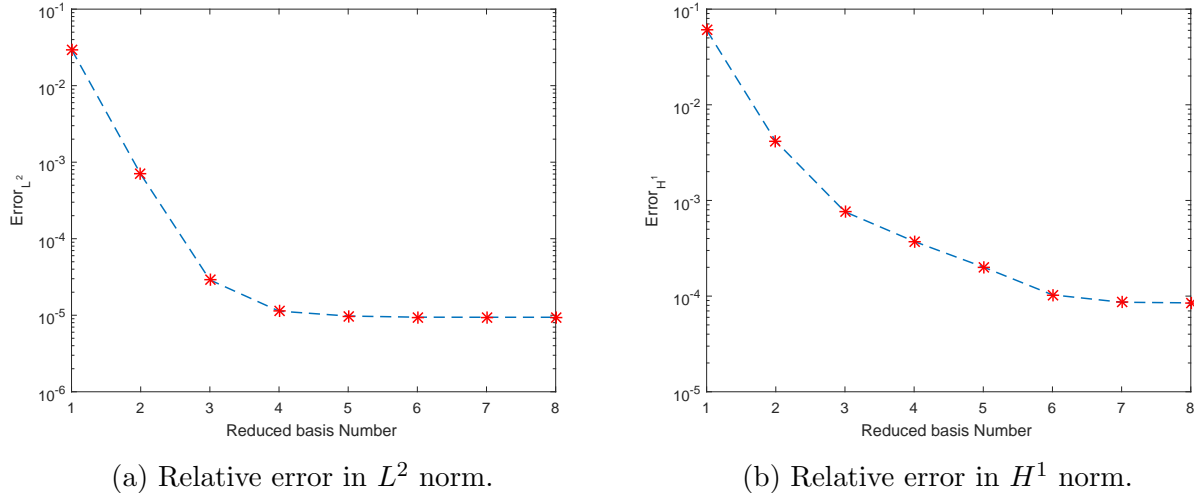


Figure 2: Relative errors with respect to the number of the multiscale reduced basis functions.

Convergence with respect to the number of qMC samples. In this numerical experiment, parameters of the random potential are the same as those in §5.1, i.e., $\sigma = 1$ and $E = [\frac{1}{9}, \frac{1}{13}, \frac{1}{11}]$. Set $\varepsilon = \frac{1}{16}$ and the final time $T = 1$. For the reference solution, we choose the meshsize to be $h = \frac{2\pi}{2048}$ and the number of qMC samples to be $n = 16000$. For our method, we choose the coarse meshsize to be $H = \frac{2\pi}{256}$ and the number of multiscale reduced basis functions to be $m_k = 4$, such that the error in the physical space be small enough. To study the convergence rate of the qMC method, we change the number of the qMC samples successively from $n = 160$ to $n = 5120$ and compute the relative L^2 errors. We also compute the relative errors of the MC method with the same setting in the physical space and the same number of samples.

In Figure 3, we show the convergence result of our method. We find that the convergence rate of the qMC method is close to $O(n^{-1})$, which is consistent with results in **Lemma 4.3** and in **Theorem 4.5**. Meanwhile, we compare the performance of the qMC method and the MC method. One can see that the convergence rate of the MC method is close to $O(n^{-\frac{1}{2}})$, which is also consistent with the error estimate of the MC method. This result clearly show that qMC method is more accurate and efficient than the MC method.

Estimation of sampling numbers in the construction of multiscale reduced basis functions. In §3.3, we obtain qualitative estimates on the choice of sampling numbers in the construction of multiscale reduced basis functions; see (25) and (26). In this experiment, we first generate Q qMC samples of the random potential: $\{v^\varepsilon(x, \omega_q)\}_{q=1}^Q$. Then, for each sample $v^\varepsilon(x, \omega_q)$, we compute the corresponding multiscale basis functions. Finally, we construct multiscale reduced basis functions using the POD method. In the online stage, we solve (32) using the obtained multiscale reduced basis functions. The numerical setting for the reference solution is the same as before. For our method, we choose $H = \frac{2\pi}{128}$, $m_k = 3$, and $n = 2560$.

In Table 2, we show relative errors of numerical solutions obtained using different sampling numbers of the random potential. When the sampling number Q is small, say $Q = 10$, the error is big and the corresponding multiscale reduced basis functions cannot approximate the

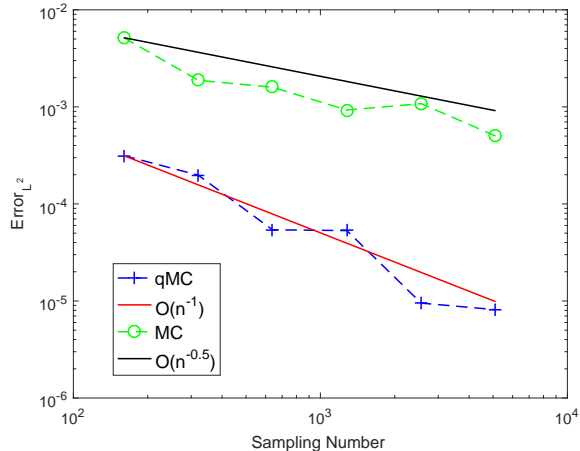


Figure 3: Comparison of the qMC method and the MC method. Convergence rate for qMC and MC are 1.13 and 0.57, respectively.

random space of the wavefunction well. When we increase Q , i.e., add more samples of the random potential in the construction of multiscale reduced basis functions, we obtain much better results. Notice that m_k is fixed to be 3. This means when Q is of order 100, the sampling number of the random potential is large enough to ensure the excellent approximation accuracy of multiscale reduced basis functions. One interesting topic on this issue is an optimal sampling strategy in the construction of multiscale reduced basis functions, which will be explored in a subsequent work.

qMC number	Error $_{L^2}$	Error $_{H^1}$
10	0.11800774	0.46614288
100	0.00136249	0.01497658
200	0.00130909	0.01455442
400	0.00129678	0.01449570

Table 2: Relative L^2 and H^1 errors in terms of sampling numbers of the qMC method in the offline stage.

Dependence of the number of qMC samples on ε and dimension of the random space m . We use the random potential $v^\varepsilon(x, \omega)$ with decaying terms satisfying **Assumption 4.4**:

$$v^\varepsilon(x, \omega) = 1 + \sum_{j=1}^m \frac{1}{j^2} \sin(jx) \xi_j(\omega) \quad (48)$$

in 1D physical domain $D = [-\pi, \pi]$ and $\xi_j(\omega)$'s are mean-zero and independent random variables uniformly distributed in $[-\sqrt{3}, \sqrt{3}]$.

Firstly, we set random dimension to be $m = 8$, the final time $T = 1$. Three values of $\varepsilon = \frac{1}{4}, \frac{1}{8}$ and $\frac{1}{16}$ are tested. The reference solution is obtained in the same way as before. For the numerical solution we use the same fine mesh as that for the reference solution but different number of qMC samples. In Table 3, we list the number of qMC samples with respect to ε

for the same accuracy requirement. It is observed that the number of qMC samples increases proportionally to $1/\varepsilon^{2.5}$.

ε	qMC number	Error $_{L^2}$	Error $_{H^1}$
1/4	160	0.00469003	0.00654782
1/8	960	0.00399369	0.00767395
1/16	5120	0.00444144	0.00785192

Table 3: Number of qMC samples for different ε under the same accuracy requirement.

Secondly, we fix $\varepsilon = \frac{1}{16}$ and change the dimension of the random space from $m = 1$, $m = 2$, $m = 4$, to $m = 8$. The reference solution and numerical solution are obtained in the same way as above. In Table 4, we list the number of qMC samples with respect to m for the same accuracy requirement. A linear growth of the number of qMC samples is observed when m is increased.

Dimension m	qMC number	Error $_{L^2}$	Error $_{H^1}$
1	520	0.00405535	0.00784524
2	1280	0.00341203	0.00667093
4	2560	0.00369911	0.00823515
8	5120	0.00444144	0.00785192

Table 4: Number of qMC samples for different dimension m under the same accuracy requirement.

A slower decay of eigenvalues in the KL expansion of the random potential requires more qMC samples. For instance, when $v^\varepsilon(x, \omega) = 1 + \sum_{j=1}^m \frac{1}{j} \sin(jx)\xi_j(\omega)$, we observed a quadratic growth of the number of qMC samples when m is increased. However, the qMC method is still very efficient in solving this difficult problem. Moreover, the qMC method can be implemented in a parallel fashion to further improve its efficiency.

5.3. Investigation of Anderson localization.

In this section, we investigate the Anderson localization phenomenon for the semiclassical Schrödinger equation using our method. Physically, when the Anderson localization happens, the electron transport stops under the strong disorder and the short-range correlation in space. We emphasize that the short-range correlation is important for localization, while the long-range correlation may lead to delocalization [14, 34]. To numerically measure the localization of a wavefunction, we define

$$A(t) = \mathbb{E} \left[\int_D |\mathbf{x}|^2 |\psi^\varepsilon(t, \mathbf{x}, \omega)|^2 d\mathbf{x} \right], \quad (49)$$

where $\mathbf{x} = x$ when $d = 1$ and $\mathbf{x} = (x_1, x_2)$ when $d = 2$.

1D Schrödinger equation. Consider the Schrödinger equation (46) with the periodic boundary condition over $D = [-\pi, \pi]$. To approximate the spatially white noise in the potential, we employ the m -term KL expansion

$$v^\varepsilon(x, \omega) = \sigma \sum_{j=1}^m \sin(jx) \frac{1}{j^\beta} \xi_j(\omega), \quad (50)$$

where $\xi_j(\omega)$'s are mean-zero and i.i.d. random variables uniformly distributed in $[-\sqrt{3}, \sqrt{3}]$. When $\beta = 0$, $v^\varepsilon(x, \omega)$ converges to the spatially white noise as $m \rightarrow \infty$. σ controls the strength of randomness.

The setup is as follows: the fine scale meshsize $h = \frac{2\pi}{600}$, the coarse meshsize $H = \frac{2\pi}{100}$, $\varepsilon = \frac{1}{8}$, $\sigma = 5$, and the initial data $\psi_{\text{in}}(x)$ is

$$\psi_{\text{in}}(x) = \left(\frac{10}{\pi}\right)^{1/4} e^{-20(x-0)^2}. \quad (51)$$

In Figure 4a, we plot $A(t)$ as a function of t for different m when $\beta = 0$. When m increases, the wavefunction quickly enters a localization phase. In Figure 4b, we plot the time evolution of $A(t)$ for different m when $\beta = 1$. Notice that $\beta = 1$ leads to a slower decay in the KL expansion of the random potential (50). Therefore, more terms need to be added to the KL expansion in order to generate a localization phase for the wavefunction. We also plot the time evolution of $A(t)$ for β ranging from 0 to 1.5 when $\sigma = 5$, $m = 15$ in Figure 5. The localization phase is much easier to be approached as β goes to 0. Besides, we also observe that a larger σ makes the wavefunction approach the localization phase more quickly with other parameters fixed. To sum up, the localization phase can be approached easier when we have more terms in the KL expansion, shorter range of randomness, or stronger randomness.

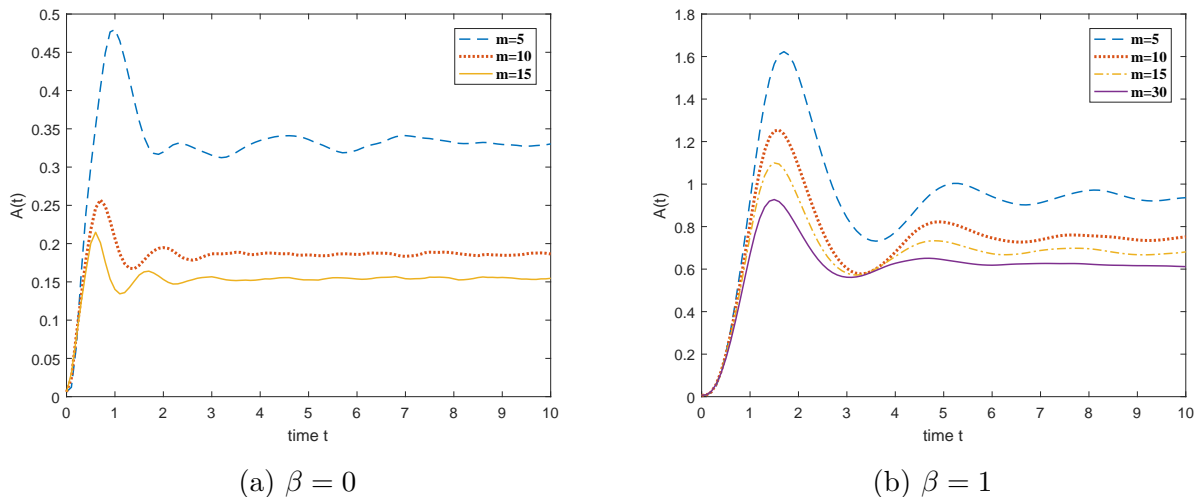


Figure 4: Anderson localization for different parameters.

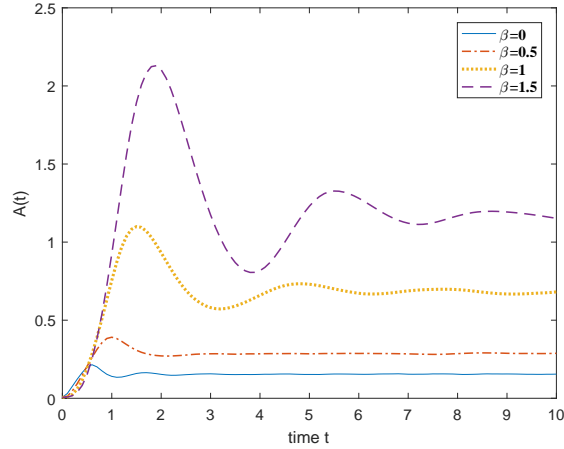


Figure 5: Anderson localization for different β .

2D Schrödinger equation. Consider the Schrödinger equation (32) over $D = [-\pi, \pi] \times [-\pi, \pi]$ and

$$v^\varepsilon(x_1, x_2, \omega) = \sigma \sum_{j=1}^m \sin(jx_1) \sin(jx_2) \frac{1}{j^\beta} \xi_j(\omega), \quad (52)$$

where the setting of $\xi_j(\omega)$'s is the same as the 1D case. σ , m and β are parameters that controls the random potential.

Choose $\sigma = 5$, $\beta = 0$ and $\varepsilon = \frac{1}{4}$. Notice that $\beta = 0$ and (52) is used to model a short-range random potential. For our method, the fine meshsize is $h = \frac{2\pi}{400}$ and the coarse meshsize is $H = \frac{2\pi}{100}$. In Figure 6, we plot the time evolution of $A(t)$ when $m = 10$. One can see that the wavefunction approaches a localization phase when $t = 4$. We remark that it is computationally expensive to solve the 2D Schrödinger equation with random potentials. The proposed method, however, is efficient to solve this problem.

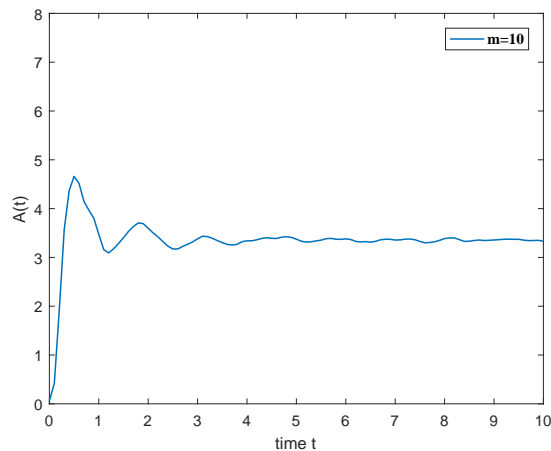


Figure 6: Anderson localization when $\sigma = 5$ and $\beta = 0$ in 2D.

6. Conclusions and discussions

In this paper, we propose a multiscale reduced basis method to solve the Schrödinger equation with random potential in the semiclassical regime. The physical space of the solution is approximated by a set of localized multiscale basis functions based on an optimization approach. The proper orthogonal decomposition method is then applied to extract a smaller number of multiscale reduced basis functions to further reduce the computational cost without loss of approximation accuracy. The number of samples to learn the multiscale reduced basis functions is also analyzed, which provides guidance in practical computations. The quasi-Monte Carlo method is employed to approximate the random space of the solution. Approximation accuracy of the proposed method is analyzed. It is observed that the spatial gridsize is proportional to the semiclassical parameter and the number of samples is inversely proportional to the same parameter. Finally we present several numerical examples to demonstrate the accuracy and efficiency of the proposed method. Moreover, we investigate the Anderson localization phenomena for Schrödinger equation with correlated random potentials in both 1D and 2D.

There are two lines of work which deserve explorations in the near future. Firstly, in the physics community, the random Schrödinger equation in higher dimensions (2D and 3D) has been frequently used to study Anderson localization; see [17] for example. Though the random potential is assumed to be white noise without spatial correlation in the original paper [2], correlated random potential is also found to generate localized states; see [10] for example. In the mathematics community, it is also known that the existence or nonexistence of Anderson localization for some types of 3D Schrödinger equations with random potentials remains open [14]. It is thus quite interesting to explore this issue from a numerical perspective. Secondly, we plan to solve the Helmholtz equation in random media using the multiscale reduced basis basis method developed in this paper.

Acknowledgements

J. Chen acknowledges the financial support by National Natural Science Foundation of China via grant 21602149. Z. Zhang acknowledges the financial support of Hong Kong RGC grants (Projects 27300616, 17300817, and 17300318) and National Natural Science Foundation of China via grant 11601457, Seed Funding Programme for Basic Research (HKU), and Basic Research Programme (JCYJ20180307151603959) of The Science, Technology and Innovation Commission of Shenzhen Municipality. Part of the work was done when J. Chen was visiting Department of Mathematics, University of Hong Kong. J. Chen would like to thank its hospitality.

References

- [1] M. AIZENMAN AND S. MOLCHANOV, *Localization at large disorder and at extreme energies: An elementary derivations*, Communications in Mathematical Physics, 157 (1993), pp. 245–278.

- [2] P. W. ANDERSON, *Absence of diffusion in certain random lattices*, Physical review, 109 (1958), pp. 1492–1505.
- [3] I. BABUSKA AND R. LIPTON, *Optimal local approximation spaces for generalized finite element methods with application to multiscale problems*, Multiscale Modeling & Simulation, 9 (2011), pp. 373–406.
- [4] W. BAO, S. JIN, AND P. A. MARKOWICH, *On time-splitting spectral approximations for the schrödinger equation in the semiclassical regime*, Journal of Computational Physics, 175 (2002), pp. 487–524.
- [5] G. BERKOOZ, P. HOLMES, AND J. L. LUMLEY, *The proper orthogonal decomposition in the analysis of turbulent flows*, Annual review of fluid mechanics, 25 (1993), pp. 539–575.
- [6] H.-J. BUNGARTZ AND M. GRIEBEL, *Sparse grids*, Acta numerica, 13 (2004), pp. 147–269.
- [7] J. CHEN, D. MA, AND Z. ZHANG, *Convergence of a multiscale finite element method for the Schrödinger equation with multiscale potentials*. In preparation.
- [8] —, *A multiscale finite element method for the Schrödinger equation with multiscale potentials*, arXiv:1901.00343, (2019).
- [9] R. DELGADILLO, J. LU, AND X. YANG, *Gauge-invariant frozen gaussian approximation method for the schrodinger equation with periodic potentials*, SIAM Journal on Scientific Computing, 38 (2016), pp. A2440–A2463.
- [10] T. DEVAKUL AND D. A. HUSE, *Anderson localization transitions with and without random potentials*, Physical Review B, 96 (2017), p. 214201.
- [11] J. DICK, F. Y. KUO, AND I. H. SLOAN, *High-dimensional integration: the Quasi-Monte Carlo way*, Acta Numerica, 22 (2013), pp. 133–288.
- [12] C. DIETRICH AND G. NEWSAM, *Fast and exact simulation of stationary gaussian processes through circulant embedding of the covariance matrix*, SIAM Journal on Scientific Computing, 18 (1997), pp. 1088–1107.
- [13] Y. EFENDIEV AND T. Y. HOU, *Multiscale finite element methods: theory and applications*, vol. 4, Springer Science & Business Media, 2009.
- [14] L. ERDOS, *Lecture notes on quantum Brownian motion*, arXiv: 1009.0843. 2010., 2010.
- [15] E. FAOU, V. GRADINARU, AND C. LUBICH, *Computing semiclassical quantum dynamics with hagedorn wavepackets*, SIAM Journal on Scientific Computing, 31 (2009), pp. 3027–3041.
- [16] E. FAOU AND C. LUBICH, *A Poisson integrator for gaussian wavepacket dynamics*, Computing and Visualization in Science, 9 (2006), pp. 45–55.

- [17] M. FILOCHE AND S. MAYBORODA, *Universal mechanism for Anderson and weak localization*, Proceedings of the National Academy of Sciences, 109 (2012), pp. 14761–14766.
- [18] J. FRÖHLICH AND T. SPENCER, *Absence of diffusion in the Anderson tight binding model for large disorder or low energy*, Communications in Mathematical Physics, 88 (1983), pp. 151–184.
- [19] R. G. GHANEM AND P. D. SPANOS, *Stochastic finite elements: a spectral approach*, Courier Corporation, 2003.
- [20] I. G. GRAHAM, F. Y. KUO, J. A. NICHOLS, R. SCHEICHL, C. SCHWAB, AND I. H. SLOAN, *Quasi-Monte Carlo finite element methods for elliptic PDEs with lognormal random coefficients*, Numerische Mathematik, 131 (2015), pp. 329–368.
- [21] T. HOU, X. WU, AND Z. CAI, *Convergence of a multiscale finite element method for elliptic problems with rapidly oscillating coefficients*, Mathematics of Computation of the American Mathematical Society, 68 (1999), pp. 913–943.
- [22] T. Y. HOU, D. MA, AND Z. ZHANG, *A model reduction method for multiscale elliptic pdes with random coefficients using an optimization approach*, Multiscale Modeling & Simulation, 17 (2019), pp. 826–853.
- [23] T. Y. HOU AND X. WU, *A multiscale finite element method for elliptic problems in composite materials and porous media*, Journal of Computational Physics, 134 (1997), pp. 169–189.
- [24] T. Y. HOU AND P. ZHANG, *Sparse operator compression of higher-order elliptic operators with rough coefficients*, Research in the Mathematical Sciences, 4 (2017), p. 24.
- [25] S. JIN, L. LIU, G. RUSSO, AND Z. ZHOU, *Gaussian wave packet transform based numerical scheme for the semi-classical Schrödinger equation with random inputs*, arXiv:1903.08740, (2019).
- [26] S. JIN, P. MARKOWICH, AND C. SPARBER, *Mathematical and computational methods for semiclassical schrödinger equations*, Acta Numerica, 20 (2011), pp. 121–209.
- [27] S. JIN, H. WU, X. YANG, ET AL., *Gaussian beam methods for the Schrödinger equation in the semi-classical regime: Lagrangian and eulerian formulations*, Communications in Mathematical Sciences, 6 (2008), pp. 995–1020.
- [28] K. KARHUNEN, *Über lineare methoden in der Wahrscheinlichkeitsrechnung*, Annales Academiae Scientiarum Fennicae, 37 (1947), pp. 1–79.
- [29] S. LI AND Z. ZHANG, *Computing eigenvalues and eigenfunctions of Schrödinger equations using a model reduction approach*, Communications in Computational Physics, (2017).

- [30] M. LOÈVE, *Probability theory. Vol. II, 4th ed. GTM. 46.*, Springer-Verlag, ISBN 0-387-90262-7, 1978.
- [31] A. MÅLQVIST AND D. PETERSEIM, *Localization of elliptic multiscale problems*, Mathematics of Computation, 83 (2014), pp. 2583–2603.
- [32] N. MOTT, *Metal-insulator transitions*, CRC Press, 1990.
- [33] F. NOBILE, R. TEMPONE, AND C. G. WEBSTER, *A sparse grid stochastic collocation method for partial differential equations with random input data*, SIAM Journal on Numerical Analysis, 46 (2008), pp. 2309–2345.
- [34] P. NOSOV, I. KHAYMOVICH, AND V. KRAVTSOV, *Correlation-induced localization*, Physical Review B, 99 (2019), p. 104203.
- [35] H. OWHADI, *Bayesian numerical homogenization*, Multiscale Modeling & Simulation, 13 (2015), pp. 812–828.
- [36] ———, *Multigrid with rough coefficients and multiresolution operator decomposition from hierarchical information games*, SIAM Review, 59 (2017), pp. 99–149.
- [37] C. SCHWAB AND R. A. TODOR, *Karhunen–Loève approximation of random fields by generalized fast multipole methods*, Journal of Computational Physics, 217 (2006), pp. 100–122.
- [38] L. SIROVICH, *Turbulence and the dynamics of coherent structures. I. coherent structures*, Quarterly of applied mathematics, 45 (1987), pp. 561–571.
- [39] N. M. TANUSHEV, J. QIAN, AND J. V. RALSTON, *Mountain waves and Gaussian beams*, Multiscale Modeling & Simulation, 6 (2007), pp. 688–709.
- [40] Z. WU AND Z. HUANG, *A Bloch decomposition-based stochastic Galerkin method for quantum dynamics with a random external potential*, Journal of Computational Physics, 317 (2016), pp. 257–275.
- [41] D. XIU AND G. E. KARNIADAKIS, *Modeling uncertainty in flow simulations via generalized polynomial chaos*, Journal of Computational Physics, 187 (2003), pp. 137–167.